Polymer 50 (2009) 261–270

Contents lists available at ScienceDirect

Polymer

journal homepage: www.elsevier.com/locate/polymer

Aggregation in dilute solutions of high molar mass poly(ethylene) oxide and its effect on polymer turbulent drag reduction

Abhishek M. Shetty*, Michael J. Solomon

Department of Chemical Engineering, University of Michigan, Ann Arbor, MI 48109, United States

ARTICLE INFO

Article history:
Received 10 August 2008
Received in revised form 15 October 2008
Accepted 18 October 2008
Available online 26 October 2008

Keywords:
Poly(ethylene) oxide
Drag reduction
Dynamic light scattering

ABSTRACT

We apply methods of dynamic light scattering (DLS) and fluid mechanics to quantitatively establish the role of aggregation in the turbulent drag reduction of high molar mass poly(ethylene oxide) (PEO) solutions. By means of DLS, we show that the dilute aqueous solutions of high molar mass PEO ($M_w \sim 4 \times 10^6$ g/mol) are aggregated and that this aggregate structure can be manipulated by addition of the chaotropic salt guanidine sulfate (GuS) or the divalent salt magnesium sulfate ($MgSO_4$). In aqueous solution, we find $\Gamma \sim q^{2.8\pm0.1}$, where Γ is the DLS correlation function relaxation rate and q is the scattering vector. This scaling is consistent with internal motions of a large coil or aggregate. Addition of salt progressively decreases the scaling to $\Gamma \sim q^{2.0\pm0.1}$ (at 0.5 M of $MgSO_4$) consistent with center-of-mass diffusion of isolated coils. We further find that manipulating the aggregation state of PEO with $MgSO_4$ shifts the critical condition for onset of turbulent drag reduction at dilute concentrations in pipe flow by a factor of 2.5. Because this critical condition is inversely proportional to the viscoelastic relaxation time of the polymer solution, we conclude that the aggregation state and the turbulent drag reduction behavior of PEO are strongly correlated. This correlation definitively confirms prior speculation (Cox et al. Nature 1974;249; Vlachogiannis et al. Physics of Fluids 2003;15(12)) that the high molar mass PEO commonly used in literature studies of turbulent drag reduction is in a state of aggregation. Furthermore, the quantitative differences in quiescent DLS characterization and turbulent flow pressure drop measurements suggest that high molar mass PEO undergoes flow-induced de-aggregation in transport systems with shear stresses as low as 0.5 Pa.

1. Introduction

Poly(ethylene oxide) (PEO) is an important commodity polymer used as a dilute additive in applications such as turbulent drag reduction, oil drilling and recovery, papermaking, wastewater treatment and drug delivery [1–7]. Fundamental understanding of PEO solution structure, dynamics and rheology may be fruitfully applied to advance these applications. However, the dilute solution properties of PEO have generated controversy because of significant differences between experimental observations and well-established classical theories of polymer science. For example the aqueous solubility of PEO is unexpected: the closest counterparts of PEO in the homologous series of polyethers, poly(methylene) oxide and poly(propylene) oxide, are both practically insoluble in water [8]. Aqueous solutions of PEO display a temperature dependence of solvent quality that is the inverse of typical polymer solvent pairs [9]. The aqueous PEO phase diagram also contains closed loop regions [10–12]. These anomalous solubility properties are a consequence of hydrogen bonding between the ether oxygen atom in PEO and the hydrogen in the water molecule [8,9,13–15].

Among the most extensively studied of the unusual properties of aqueous PEO solutions is its clustering behavior. It has been reported that, above a critical concentration that is molecular weight dependent, polymer clusters (or aggregates) coexist in equilibrium with free polymer coils [16]. Others have found that, at concentrations much below the critical overlap concentration (c^*), PEO exists as two phases, each with different polymer concentration. The polymer rich phase of these two has been reported to organize into a liquid–crystalline fibrillar network that leads to properties such as shear thinning and elasticity [17].

Aggregation of PEO in solution has been studied by electron microscopy, dynamic light scattering (DLS), static light scattering (SLS) and small-angle neutron scattering (SANS) [16,18,19]. Electron micrographs of dilute solutions of PEO in dimethylformamide and water solutions subjected to drying revealed supermolecular structures that were much larger than the molecular dimensions of PEO [18,20]. DLS of dilute solutions of PEO in methanol yielded intensity autocorrelation functions

* Corresponding author. Department of Chemical Engineering, University of Michigan, 2300 Hayward Street, 3074 H.H Dow Building, Ann Arbor, MI 48109, United States.
E-mail addresses: amshetty@umich.edu (A.M. Shetty), mjsolo@umich.edu (M.J. Solomon).

0032-3861/$ – see front matter © 2008 Elsevier Ltd. All rights reserved.
doi:10.1016/j.polymer.2008.10.026

consistent with two relaxation times. The ability of low molecular weight PEO used in the study to form clusters depended on the history of the sample and the temperature used. The fast relaxation mode was attributed to the well-solvated dispersed monomolecular species and the slow relaxation mode was caused by the formation of aggregates in solution [21]. Both relaxation modes (as characterized by a relaxation rate, Γ) scaled with the scattering vector, q, $\Gamma \sim q^2$, consistent with polymer center-of-mass diffusion [22].

Zimm plot analysis of SLS measurements of dilute PEO solutions has revealed curvature at low angles [10,23]. Such curvature is thought to be a very sensitive indicator of aggregation in solution [24]. Hammouda et al. recently concluded from SANS measurements that hydrogen bonding and hydrophobic interactions in PEO/water systems have a primary role in the formation of aggregates [19]. They observed two correlation lengths in the SANS scattering spectrum. The long range correlation was due to clustering and the short range one was due to single polymer chains [19,25].

The unusual rheology of dilute aqueous solutions of PEO has also been taken as evidence for presence of aggregates [26,27]. (Here we define an aggregate in a dilute solution is a polymer structure comprised of more than one molecular chain, but which is not a sample spanning network or gel.) Dilute linear (Zimm and Rouse) and non-linear bead spring (FENE) constitutive polymer models, which are based on parameters such as the molar mass of a single polymer chain and polymer contour length, fail to capture the rheological behavior of these solutions. For example, from measurements of capillary filament breakup, Tirtaatmadja et al. have reported that the structure of high molar mass PEO at ~10–100 ppm concentrations is not consistent with the prediction of the Zimm model [28].

An important feature of dilute aqueous solutions of high molar mass PEO is their ability to reduce friction drag in flow. It is well known that the addition of a small amount of high molar mass polymer to a turbulent Newtonian fluid flow results in drag reduction [29,30]. High molecular weight PEO is the most commonly used polymer for turbulent drag reduction in aqueous solutions since significant drag reduction can be achieved at very small concentrations [31,32]. However, the drag reduction capacity of dilute PEO appears to be much greater than predicted by dilute solution constitutive equations [33].

The role of PEO aggregation in turbulent drag reduction can be indirectly inferred from literature measurements. For example, viscoelastic relaxation times extracted from measurements of the onset shear stress of turbulent drag reduction in pipe flow do not agree with estimates for single molecules of PEO, as computed from the Zimm model [33]. (This assignment is possible because the onset condition for turbulent drag reduction is inversely proportional to the solution viscoelastic relaxation time [34].) Second, Dunlop and Cox concluded that molecular aggregates exist in dilute PEO solutions by monitoring the rate of change of torque with time in a spinning disk apparatus [35]. Third, Liberatore et al. and Vlachogiannis et al. inferred the presence of aggregates in PEO solutions by showing that loss of turbulent drag reduction with time in PEO solutions was not related to the reduction in molecular weight of the solutions due to scission [36,37]. Fourth, by means of small-angle light scattering (SALS) and rheoptics, Liberatore et al. observed signatures of structural heterogeneities in PEO solutions under shear which are attributed to polymer aggregation [38,39]. Further support for the effect of aggregation on PEO drag reduction comes from direct numerical simulation. Far greater magnitudes of the polymer relaxation time have been required to model the turbulent statistics and onset phenomena of turbulent drag reduction that could be supported by single chain theories of polymer dynamics [40].

However, because experiments have yet to directly probe molecular structure and turbulent flow behavior in the same PEO system, the experimental evidence for a role of aggregation in PEO turbulent drag reduction is indirect. A direct approach to link aggregation with the drag reduction behavior of PEO would be to disrupt aggregate structure in a polymer of a particular molar mass through the effect of an additive. Such additives exist: Little and coworkers have studied the effect of salts like magnesium sulfate and potassium carbonate on the turbulent drag reduction of PEO [41,42]. They show that progressive addition of salt decreases the drag-reducing tendency of these solutions. Yuan and coworkers have likewise demonstrated that such salts can be used as an agent to disrupt hydrogen bonding capability in aqueous soluble polymers such as poly(N-isopropylacrylamide) [43]. Lim and coworkers have found that addition of salts shifts the theta point, T_θ, of polymer–salt mixtures, which in turn has an effect on their drag reduction characteristics [44]. Based on these observations, we hypothesized that divalent and/or chaotropic salts might be a suitable method to disrupt the aggregate structure of PEO. At concentrations ~0.1–1.0 M, chaotropic salts disrupt local water structure and are perhaps best known for their role as agents of cell lysis and protein denaturation [45].

The approach of this work is to systematically create different polymer aggregation states in the same polymer system by addition of the salts discussed above. Subsequently, using these polymer states, we examine the aggregate structure (by DLS) and flow behavior (by drag reduction measurements) of dilute PEO solutions. This approach is motivated by recent findings of difficulty in characterizing the molecular structure of high molar mass PEO solutions by means of static light scattering (SLS). In particular, SLS of dilute high molar mass PEO conducted in conjunction with gel permeation chromatography failed to yield reproducible characterization of the molar mass and radius of gyration [46]. We therefore used dynamic light scattering to characterize quiescent aggregation of high molar mass PEO.

The organization of the paper is as follows. We first present DLS results of high molar mass PEO solutions in deionized water that are consistent with the dilute aggregate hypothesis. Next, we show that the salts magnesium sulfate and guanidine sulfate change the aggregate structure of dilute PEO solutions. We then demonstrate the significant effect of aggregate structure on the drag-reducing tendency of these solutions by comparing results of the DLS studies with parallel studies of turbulent drag reduction.

2. Experimental section

2.1. Materials

Two different grades of high molar mass poly(ethylene oxide) (PEO) were used in this study. The first is a polydisperse PEO with manufacturer reported molar mass $M_w \sim 4 \times 10^6$ g/mol (WSR 301, Dow Chemicals; $M_w/M_n > 20$ [47]). The second is a PEO of different weight-average molar mass and more narrow molar mass distribution (PEO – 1182 K, Polymer Laboratories, $M_w = 1.2 \times 10^6$ g/mol; $M_w/M_n = 1.12$). The overlap concentrations, c^* as determined by the measurement of intrinsic viscosity (data not shown) are 620 ppm and 2600 ppm respectively. Dilute solutions of these polymers were prepared with HPLC grade water (Sigma Aldrich, for light scattering measurements) and with deionized water (for turbulent drag reduction experiments) from stock solutions. To prevent shear degradation, polymer solutions were prepared in 0.1 L (for light scattering) and 1 L (for drag reduction) bottles placed on rollers (Wheaton Science Products) rotating at 3–6 rpm for ~24–48 h. The salts guanidine sulfate (GuS, Sigma Aldrich) and magnesium sulfate ($MgSO_4$, Sigma Aldrich) were prepared in the concentration range

0.1–1.0 M. Experiments were performed within 3–4 days after dilution to minimize any possible degradation due to aging.

2.2. Dynamic light scattering (DLS)

DLS was performed on a compact goniometer system (ALV, Langen, Germany) equipped with a multi-tau digital correlator (ALV-5000E, Langen, Germany). The minimum delay time of the correlator used was 12.5 ns. A Laser source with wavelength of $\lambda_0 = 488$ nm (Innova 70C, Coherent Inc., Santa Clara, CA) was used. Measurements were done in the angular range $\theta = 20$–115° ($5.94\ \mu m^{-1} < q < 28.86\ \mu m^{-1}$) so as to span at least a decade in q, the scattering vector, where $q = 4\pi n \sin(\theta/2)/\lambda_0$. Here n is the refractive index of the solvent, λ_0 is the wavelength of incident light source and θ is the scattering angle. All measurements were done at $T = 298 \pm 0.5$ K. The sample vials used were cleaned by first sonicating them in acetone for about an hour, drying them overnight and then subjecting them to UV ozone treatment (UVO cleaner, Jelight, Irvine, CA) to ensure that they were free from any organic residue. The polymer and salt solutions prepared were filtered using a 1.5 μm filter (Whatman 25 mm GD/X syringe filters) prior to DLS measurements.

2.3. Turbulent drag reduction characterization

Polymer turbulent drag reduction is a sensitive function of the molecular structure of the drag-reducing additive. The pipe flow experiment for characterization of polymer turbulent drag reduction has been previously described [48]. The apparatus has the following capabilities: First, to access the very low wall shear stresses ($\tau_w \sim 0.5$–1 Pa) associated with the onset of turbulent drag reduction in high molar mass aggregated PEO solutions, a test section consisting of 1/2 inch diameter stainless-steel pipe was used. Second, to access the small pressure drops associated with low wall shear rates, a highly sensitive differential pressure transducer (GP50, Grand Island, NY, range 0–0.18 psi) was used. Pressure drop measurements were performed across a test section 0.7 m long. The pressure transducer responses were acquired via a National Instruments LABVIEW data acquisition system (Model USB-6009). Since fully developed flow is more difficult to realize in polymer solutions than in Newtonian fluids, a large entrance length ($L/D = 290$) was incorporated prior to the test section [49]. We found that no static pressure correction was required in our pressure drop measurements due to the relatively low Reynolds number ($\sim 10^4$) of the experiments [50].

As per the review of Virk [34], the standard data analysis method to characterize polymer drag reduction is the Prandtl–von Karman plot. Molecular properties of the dilute polymer solution such as concentration and molecular size affect the pressure drop – volumetric flow rate properties of turbulent pipe flow. In dimensionless form, the pressure drop is quantified by the friction factor, f. The volumetric flow rate is quantified by the Reynolds number, Re. Here, $f = 2\tau_w/U_{av}^2\rho$, where τ_w is the wall shear stress, U_{av} is the mean fluid velocity in the flow direction averaged across the pipe's cross-section and $\mathrm{Re} = dU_{av}/\nu_s$, where d is the pipe diameter and ν_s is the kinematic viscosity of the fluid. The wall shear stress is related to the pressure drop: $\tau_w = \Delta P d/4L$, where ΔP is the pressure drop across a test section of length L. In the Prandtl–von Karman plot [34], the axes are $1/\sqrt{f}$ (ordinate) and $\mathrm{Re}\sqrt{f}$ (abscissa).

3. Results

3.1. DLS of dilute aqueous solutions of PEO

Typical measurements of the $g_2(\tau)$ for a 20 ppm ($c/c^* \sim 0.03$) aqueous solution of PEO WSR 301 over a range of scattering angles are plotted in Fig. 1a. The normalized intensity autocorrelation function, $g_2(t) = \langle I(t)I(0)\rangle/\langle I\rangle^2$ is an exponentially decaying function in dilute solution:

$$g_2(t) = A\exp(-2\Gamma t) = A\exp(-2t/\tau) \quad (1)$$

Here Γ is the previously described DLS relaxation rate, inversely related to the DLS relaxation time, τ, of the polymer and A is a constant that takes into account deviations from ideal correlation. Both quantities are q-dependent. The probability distribution of the relaxation time spectra was obtained by a CONTIN (constrained regularization) deconvolution of the correlation functions [51]. (Other means of analysis, such as the method of cumulants, yield

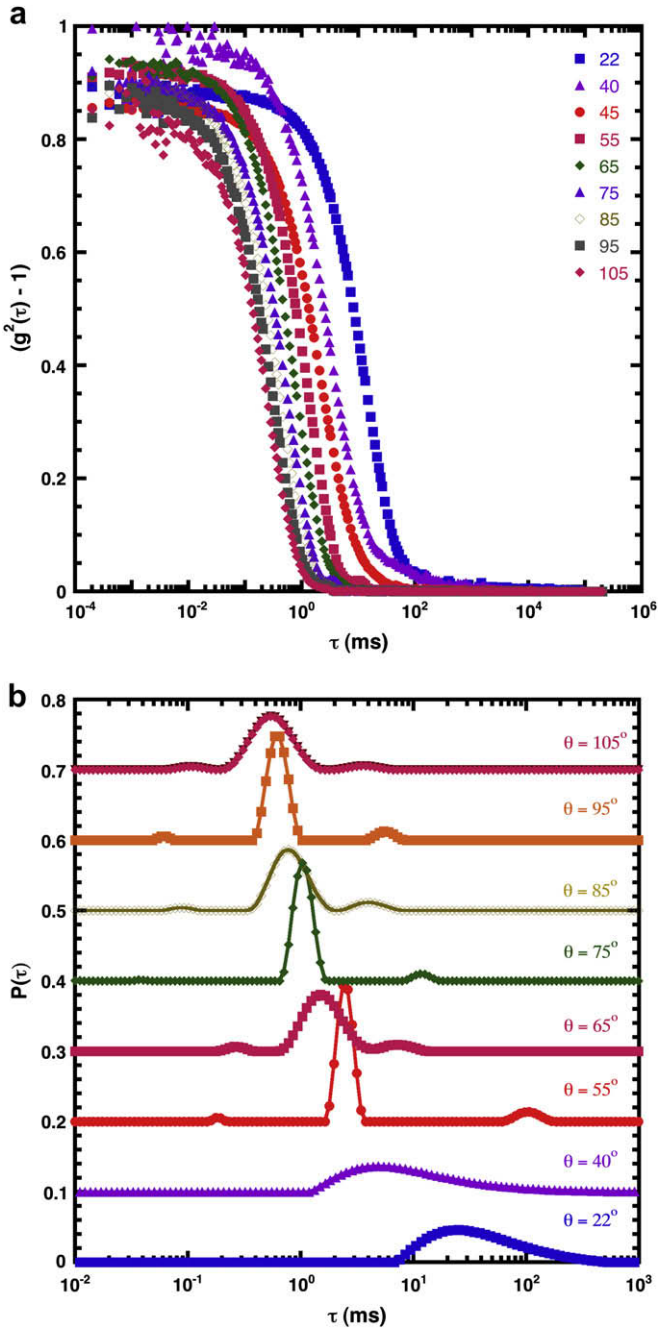

Fig. 1. (a) Intensity autocorrelation function $g_2(\tau)$ for 20 ppm ($c/c^* \sim 0.03$) PEO WSR-301 as a function of scattering angle, θ. (b) Probability distribution function of the DLS decay time spectrum for 20 ppm PEO WSR-301, obtained from CONTIN deconvolution of $g_2(\tau)$ reported in Fig. 1(a).

analogous results.) Fig. 1b reports the probability distribution function of the CONTIN relaxation time spectrum measured for a typical duration of 600 s. (The very small additional modes detected by CONTIN at higher angles are either spurious or due to dust. No systematic trend in these small amplitude modes was detected over the full range of scattering angles studied.)

The q-dependence of the DLS relaxation rate at dilute concentrations of PEO WSR-301 as obtained by CONTIN deconvolution is plotted in Fig. 2a. CONTIN analysis of the measured $g_2(t)$ yielded a dominant single-mode relaxation at all conditions and it is this peak which is plotted. The data show negligible dependence on polymer concentration over the 5–50 ppm range studied. Thus, these measurements are in the dilute regime, consistent with the measured overlap concentration, $c^* = 620$ ppm. Further results reported are in this dilute range.

In Fig. 2a power law scaling of the measured relaxation rate Γ with q is not consistent with center-of-mass diffusion of a single-polymer coil (where Brownian motion of the entire polymer coil is measured). For a dilute polymer system, in the limit $qR_h \ll 1$, $\Gamma = Dq^2$, where D is the self-diffusion coefficient of the polymer coil [22]. Instead, a power law fit to Fig. 2a data yields $\Gamma = 1.47 \times 10^{-18} q^{2.8\pm0.1}$. We conclude that the q range of our instrument, 5.94 $\mu m^{-1} < q < 28.86\ \mu m^{-1}$, is not such that $qR_h < 1$. In fact, from published correlations, we predict the single molecule $R_h \sim 85$ nm for the PEO studied in Fig. 2a, a size for which $qR_h \sim 1$ [52] ($qR_h = 0.5$ at $\theta = 20°$).

To explain this result, consider the dynamic response of a polymer chain in the $qR_h \gg 1$ limit for the Zimm model in a good solvent is $\Gamma = 0.07kTq^3/\eta$, where η is the solvent viscosity, k is the Boltzmann constant and T is the temperature [22]. The predicted $\Gamma \sim q^3$ scaling has been previously observed by Adam and Deslanti for dilute solutions of very large ($M_w = 24 \times 10^6$ g/mol) polystyrene molecules in benzene [53]. The scaling exponent of three reflects internal fluctuations of the polymer coil with inclusion of hydrodynamic interactions.

Based on these previous observations for large single chains, we hypothesize that the unusual scaling reported in Fig. 4a is due to the effect of internal fluctuations of large polymer aggregates. That is, if WSR-301 aggregates to the extent that Fig. 2a measurements are in the regime $qR_{h,agg} \gg 1$, then the scaling of (Fig. 2a) could be explained by the Zimm model result $\Gamma \sim q^3$. This hypothesis implicitly assumes that internal fluctuations of large polymer aggregates and large single polymer chains yield comparable DLS relaxation spectra.

The magnitude of the power law prefactor in Fig. 2a is 1.47×10^{-18}. The Zimm model theory for internal fluctuations predicts a prefactor magnitude of 3.24×10^{-19} and 2.77×10^{-19} for a theta and good solvent, respectively (for the viscosity of H_2O at $T = 298$ K). Thus, although the q^3 scaling of Fig. 2a agrees well with the aggregate hypothesis, the prefactor differs significantly from the Zimm theory.

Other potential explanations of Fig. 2a results are not consistent with the data. For example, the results are not explained by the semi-dilute dynamics of flexible polymer solutions because in the semi-dilute regime bimodal relaxation behavior is observed [22,54]. Moreover, both relaxation modes in semi-dilute solutions

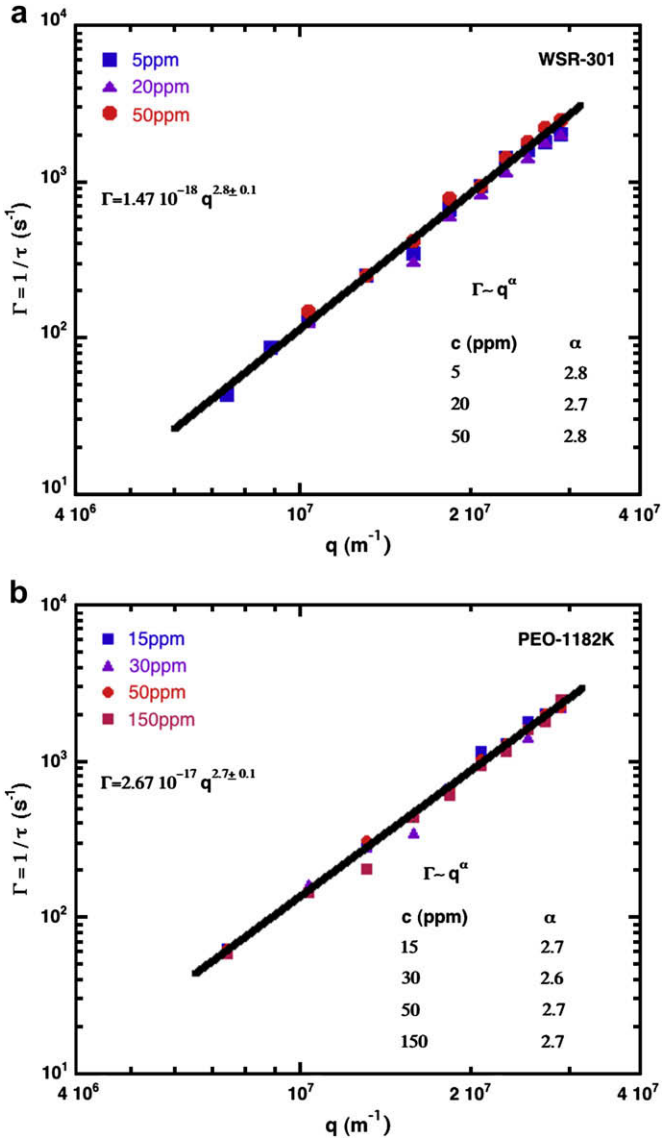

Fig. 2. (a) Peak relaxation rate, Γ, from CONTIN deconvolution as a function of the scattering vector q for different dilute concentrations (5–50 ppm) of PEO WSR-301. (b) Peak relaxation rate, Γ, from CONTIN deconvolution as a function of the scattering vector q for different dilute concentrations (15–150 ppm) of narrow polydisperse PEO-1182 K ($M_w \sim 1.2 \times 10^6$ g/mol, $M_w/M_n \sim 1.12$).

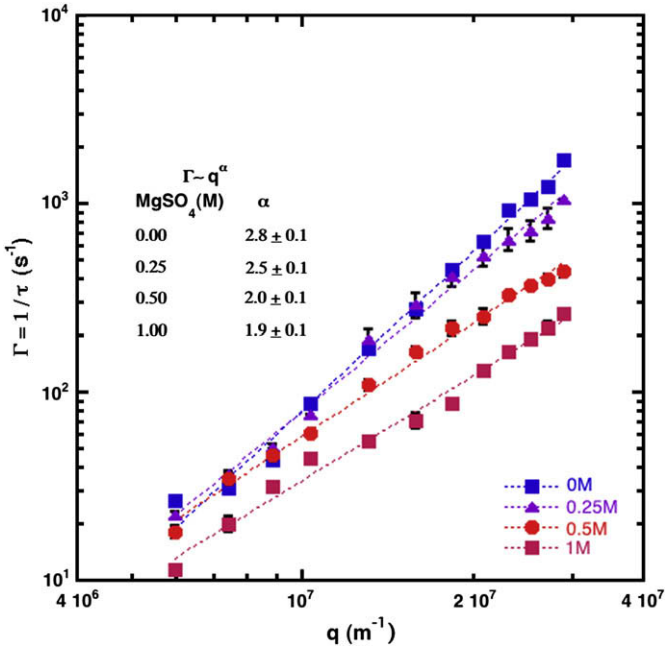

Fig. 3. The effect of $MgSO_4$ concentration on the q-dependence of the peak relaxation rate Γ at 5 ppm for PEO WSR-301.

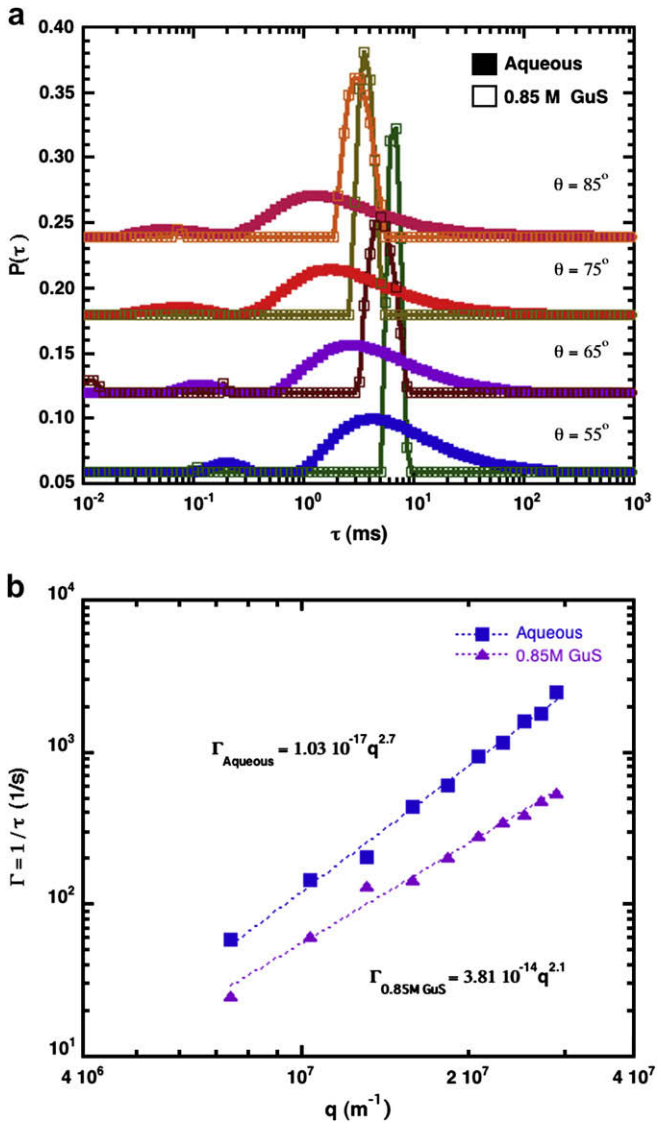

Fig. 4. (a) Comparison of the DLS decay time spectrum for 150 ppm narrow polydisperse PEO-1182 K ($M_w \sim 1.2 \times 10^6$ g/mol, $M_w/M_n \sim 1.12$) in deionized water (aqueous) and with guanidine sulfate salt (0.85 M GuS) at different scattering angles. (b) Peak decay relaxation rate, Γ, as a function of q for the deionized water (aqueous) and guanidine sulfate salt (0.85 M GuS) case (150 ppm narrow polydisperse PEO-1182 K).

show $\Gamma \sim q^2$ scaling [55,56]. Another potential explanation of the data could be the effect of chain stiffness. Harnau and coworkers investigated the effect of chain stiffness on the relaxation rate scaling (Γ) for dilute semi-flexible polymers and found a characteristic $\Gamma \sim q^{8/3}$ scaling [57]. However, this behavior was observed only at large scattering vectors $q/2p > 1.5$, where $1/2p$ is the persistence length of the polymer chain. The $q/2p$ values probed in our experiments (0.003–0.016) are more than an order of magnitude lower than this bound. Thus, semi-flexible polymer dynamics is not an explanation for our experimental observations. Moreover, our results cannot be explained by rigid rod theory, since rod-like chains exhibit $\Gamma \sim q^2$ scaling [58]. Finally, very recent measurements at large scattering vectors on microgels of highly swollen flexible crosslinked polymer chains displayed a scaling ($\Gamma \sim q^3$) similar to our findings [59]. Although the coincidence of these two scalings suggests a potential relationship between structural descriptions based on the concepts of microgels and aggregates, further understanding of this correspondence is not available at this time.

To address if the findings are sensitive to a difference in the M_w and M_w/M_n of PEO, DLS of dilute solutions of PEO with $M_w = 1.2 \times 10^6$ g/mol and $M_w/M_n = 1.12$ was performed. The best-fit of the data for this polymer is $\Gamma = 2.67 \times 10^{-17} q^{2.7 \pm 0.1}$ (Fig. 2b), consistent with the results of Fig. 2a. Thus, the q^3 scaling characteristic of internal dynamics is not sensitive to this change in molar mass and M_w/M_n. In addition, the scaling prefactor is a function of extent of polydispersity and/or molar mass, since it changes by about a factor of ten between the two polymers.

3.2. Manipulation of PEO aggregate structure with addition of salt

Fig. 3 reports the q-dependence of single relaxation rate peak of a 5 ppm solution of WSR-301 (polydisperse; $M_w \sim 4 \times 10^6$ g/mol) for $MgSO_4$ added at concentrations of 0.25 M, 0.5 M and 1.0 M. Salt free data from Fig. 2a are also plotted for reference. The figure shows that the relaxation rates scale as a power law for all $MgSO_4$ concentrations. The magnitude of the scaling exponent monotonically decreases with salt concentration from 2.8 ± 0.1 for salt free solutions to 1.9 ± 0.1 for 1.0 M $MgSO_4$ additives (errors reported are standard error of the mean of three replications of the curves).

Recall the two limiting cases for the DLS relaxation spectrum of dilute solutions: In the limit $qR_h \ll 1$, $\Gamma \sim q^2$, reflecting center-of-mass diffusion; for $qR_h \gg 1$, $\Gamma \sim q^3$, reflecting internal coil dynamics. Thus, the likely interpretation of Fig. 3 is that the addition of salt shifts the DLS relaxation spectrum between these two limits. To yield the shift in limits, addition of salt could destroy the aggregate structure found in aqueous solution. As the balance between aggregates and single chains shifts, R_h decreases, and the change in limiting scaling behavior is realized.

To check this interpretation, we compute an effective R_h from the diffusive scaling at high salt concentrations, and assess whether this R_h is consistent with the expected dimensions of high molar mass PEO. Here, $R_h = k_b T/6\pi\eta D$ where η is the viscosity of the salt solution (measured by capillary viscometry to be 0.00133 Pa s). By this method, $R_h \sim 290$ nm for WSR 301 in 0.5 M $MgSO_4$. This value of R_h is large – corresponding to an effective molar mass $\sim 3 \times 10^7$ g/mol – and is thus on the boundary of a physically realistic value. It perhaps indicates that PEO in salt solution still comprises some residual aggregate character. Nevertheless, the key

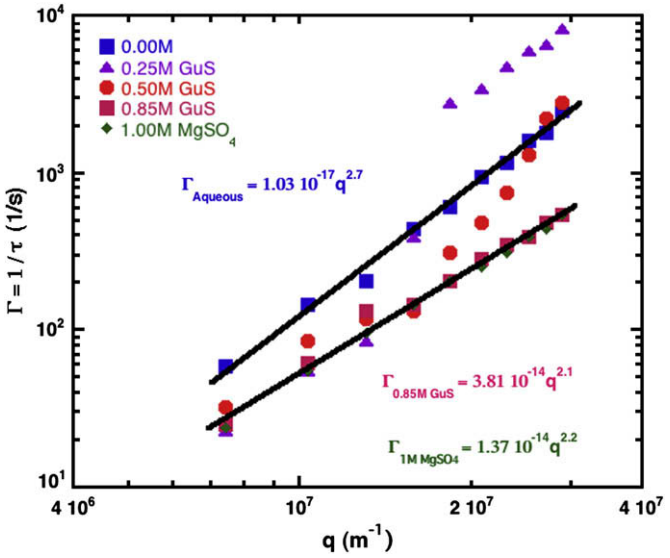

Fig. 5. Effect of guanidine sulfate salt (GuS) concentration and 1 M magnesium sulfate ($MgSO_4$) on the q-dependence of Γ for narrow polydisperse aqueous PEO-1182 K (150 ppm).

finding is that the addition of salt decreases the effective size of WSR 301 into a range where its center-of-mass diffusion can be measured by DLS. (Note that R_h can be estimated only for solutions for which the relationship $\Gamma = (k_bT/6\pi\eta R_h)q^2$ is satisfied. Only the data for the highest salt concentrations of Fig. 3 satisfy this relationship.)

Fig. 4a compares the DLS relaxation spectrum for a different PEO (150 ppm, $M_w \sim 1.2 \times 10^6$ g/mol; $M_w/M_n = 1.12$) in salt-free and 0.85 M GuS solutions. Although both solutions yield only a single dominant relaxation peak, the peaks are significantly broader for the aqueous solution than for the salt solution. The q-dependence of this change is plotted in Fig. 4b. The results for this polymer/salt pair are consistent with Fig. 3: the relaxation rate scaling shifts from one indicative of aggregate dynamics ($\Gamma \sim q^{2.7}$) to one characteristic of polymer center-of-mass diffusion ($\Gamma \sim q^{2.0}$). Thus, Fig. 3 results are not specific to the particular polymer/salt pair studied.

Thus, the data of Figs. 3 and 4 are consistent with the hypothesis that the salts GuS and $MgSO_4$ disrupt PEO aggregate structure in dilute solution, thereby yielding a solution of single coils. Additional experiments (Fig. 5) explored the intermediate salt concentration range for GuS at 0.25 M and 0.5 M and found that at these conditions Γ displays a complex q-dependence that cannot be described by a power law scaling. Nevertheless, power law scalings with well-characterized exponents are obtained in the high salt limit of 0.85 M GuS and 1 M $MgSO_4$. Using the Stokes–Einstein equation we find the effective R_h from the diffusive scaling at high salt concentrations for PEO with $M_w \sim 1.2 \times 10^6$ to be 185 nm and 189 nm in 0.85 M GuS and 1 M $MgSO_4$ respectively.

3.3. *Effect of aggregate structure on turbulent drag reduction studied by addition of $MgSO_4$*

Fig. 6 reports drag reduction measurements for different concentrations of WSR-301 as a Prandtl–von Karman plot, generated by the procedure described in the methods. The data from which the plot was generated are shown in the inset of the figure. The lower solid line in Fig. 6 is the Prandtl–von Karman (PK) curve – the friction drag for a Newtonian fluid – and the upper solid line is the maximum drag reduction asymptote (MDR) – an (empirical) upper bound for friction drag reduction in polymer flows [34]. (The performance of the device over the conditions of interest ($400 < \mathrm{Re}\sqrt{f} < 1000$) was verified by measurements with water. As shown in Fig. 6, the results for water agree well with the Newtonian result, the PK line.)

In Fig. 6, polymer data deviate from the PK curve once a critical wall shear rate τ_w^* is reached. Above this point, friction drag is lower, and the polymer curve increasingly deviates from this curve. Virk discusses that τ_w^* is determined by a critical Weissenberg number (Wi^*). Wi^* depends on polymer variables: $Wi^* = \lambda\tau_w^*/\mu$, where λ is the relaxation time of the polymer, τ_w^* is the onset wall stress and μ is the viscosity of the solvent [34]. Wi^* can be predicted from Virk; $Wi^* = 1.6$ for the polymer studied in this work. The interested reader is referred to Appendix for additional details of polymer drag reduction phenomenology and data analysis.

Fig. 7 compares the turbulent drag reduction behavior of the high molar mass polymer WSR 301 in salt free and 0.5 M $MgSO_4$ at the dilute concentrations of 2, 5 and 25 ppm. Based on the DLS results these measurements compare the behavior of aggregated (aqueous) and de-aggregated (0.5 M $MgSO_4$) PEO. The onset wall shear stress, τ_w^*, for polymer drag reduction is estimated by a linear extrapolation of the polymer curve [as per Eq. (2) (Appendix)] to its intersection with the PK curve. (Linear extrapolation on a Prandtl–von Karman plot to characterize the onset condition is standard in the fluid dynamics literature [34,48].) The slope increment, δ, quantifies the difference between the slopes of the polymer and Newtonian data. It was determined for each solution by a least-squared fit to the data, as per Eq. (2). Table 1 reports the onset stress (τ_w^*) and slope increment (δ) for the different polymer and salt concentrations from Fig. 7. Errors in the table were estimated by unweighted least square fit analysis. The table shows a significant effect of salt, and thus aggregate structure, on both these quantities.

Fig. 8 plots the onset stress conditions from Fig. 7 and Table 1 as a function of polymer concentration. Plotted also is the predicted onset wall shear stress for WSR 301 given the assumption of unaggregated, single-molecule behavior. (This prediction is computed from the correlation, $R_g^3\tau_w^* = \Omega_T$, for onset of polymer drag reduction given by Virk [34]. Here R_g is the radius of gyration for the polymer, as estimated from published correlations for PEO [52], and Ω_T is an average onset constant for PEO. As given in Virk $\Omega_T = 4.4 \times 10^6$). Error bars plotted for the onset stress are from the unweighted least square fit analysis, as in Table 1.

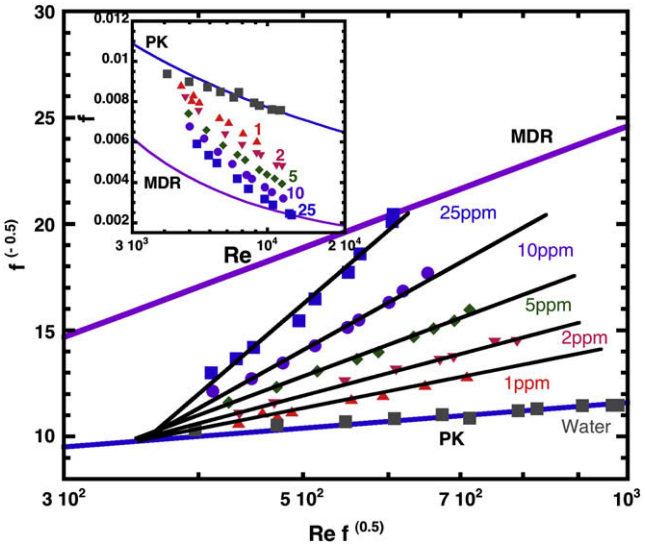

Fig. 6. Prandtl–von Karman plots for different PEO WSR-301 concentrations ranging from 1 to 25 ppm. As discussed in the text, the lower curve is the Prandtl–von Karman (PK) law for a Newtonian solvent and the upper curve is the maximum drag reduction asymptote for polymer turbulent drag reduction. The inset plot is a f vs Re plot for the different PEO WSR-301 concentrations studied above.

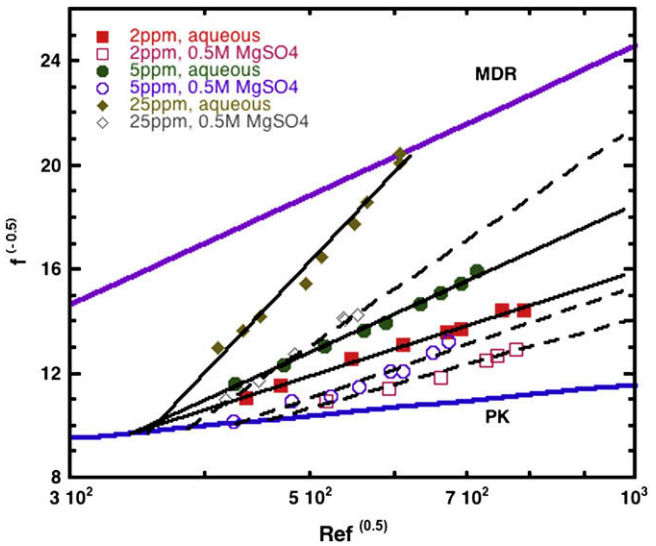

Fig. 7. Effect of magnesium sulfate (0.5 M $MgSO_4$) addition on the turbulent drag reduction behavior of dilute PEO WSR-301 solutions.

Table 1
Onset stress (τ_w^*) and slope increment (δ) values obtained from drag reduction measurements for the different polymer and salt concentrations used in the study.

Concentration (ppm) WSR-301	Onset stress, τ_w^* (Aqueous)	Onset stress, τ_w^* (0.5 M $MgSO_4$)	Slope increment, δ (Aqueous)	Slope increment, δ (0.5 M $MgSO_4$)
1	0.54 ± 0.15	1.34 ± 0.15	9.9 ± 0.76	8.4 ± 0.8
2	0.52 ± 0.14	1.53 ± 0.18	13.4 ± 0.56	11.4 ± 1.15
5	0.52 ± 0.16	1.39 ± 0.33	19 ± 0.72	14.6 ± 2.15
10	0.53 ± 0.3	1.03 ± 0.14	28.1 ± 1.6	18.2 ± 1.12
25	0.53 ± 0.24	1.08 ± 0.18	44 ± 2.26	28 ± 1.63

Fig. 8 shows that the pipe flow experiments of aqueous (salt free) WSR-301 solutions yield significantly different drag reduction behavior relative to the single-molecule prediction. If the salt-free measurements were explained by single-molecule behavior, the effective molar mass of WSR 301 would be estimated to be $\sim 7 \times 10^6$ g/mol, not too different from the manufacturer's estimate of 4×10^6 g/mol, especially in light of the significant polydispersity ($M_w/M_n > 20$) of the polymer. However, this effective molar mass is entirely inconsistent with the q^3 scaling of the aqueous DLS relaxation rates reported earlier. That is, if the quiescent molar mass of WSR 301 was indeed $\sim 7 \times 10^6$ g/mol, then we would predict $R_h \sim 117$ nm, a value characterizable by DLS, as well as consistent with the observation of a q^2 scaling of the polymer relaxation rate, rather than the measured q^3 dependence.

The difference between the DLS and turbulent drag reduction data is likely explained by a role for flow-induced de-aggregation of WSR-301 in the turbulent pipe flow experiments. If the Re $\sim 10^4$ flow breaks down aggregate structure of quiescently aggregated solutions, then the effective single-molecular behavior of Fig. 8 is explained. Because the effect of de-aggregation is apparent as the onset condition, its effect is already significant in the piping system for flows as weak as $\tau_w \sim 0.5$ Pa.

For the 0.5 M $MgSO_4$ solutions, the observed behavior is much closer to the single-molecule prediction. To address if the results could be explained by a change in solvent quality from good (salt free) to theta (0.5 M $MgSO_4$), we performed the following analysis: From the Zimm bead spring theory for single polymer chains, the relaxation time $\lambda \sim [\eta]\eta_s M/RT$, where η_s is the solvent viscosity, R is the ideal gas constant, T is the absolute temperature and $[\eta]$ is the intrinsic viscosity of the polymer. In a good solvent system, $[\eta] \sim M_w^{0.8}$ and for a theta solvent, $[\eta] \sim M_w^{0.5}$ (from Mark–Houwink equation) [60]. Based on the critical Weissenberg number, Wi^* [61–63], for onset of polymer drag reduction given by Virk [35], $Wi^* = \lambda\tau_w^*/\mu$, we estimate $\tau_{w,T}^*/\tau_{w,G}^*$, where the subscripts T and G indicate a theta (PEO-0.5 M $MgSO_4$) and good solvent (PEO-salt free) respectively. We compute this ratio to be 1.5, which is less than the experimentally observed ratio of 2.5. Thus, we conclude that the differences in Fig. 8 are not simply a consequence of solvent quality effects. Moreover, although turbulent drag reduction and DLS are sensitive to different moments of the molar mass distribution, this sensitivity does not explain the large effect of salt observed in Fig. 8. Because salt does not change the molar mass distribution of the polymer, the salt effects are most likely a consequence of changes in aggregation or susceptibility to flow-induced de-aggregation.

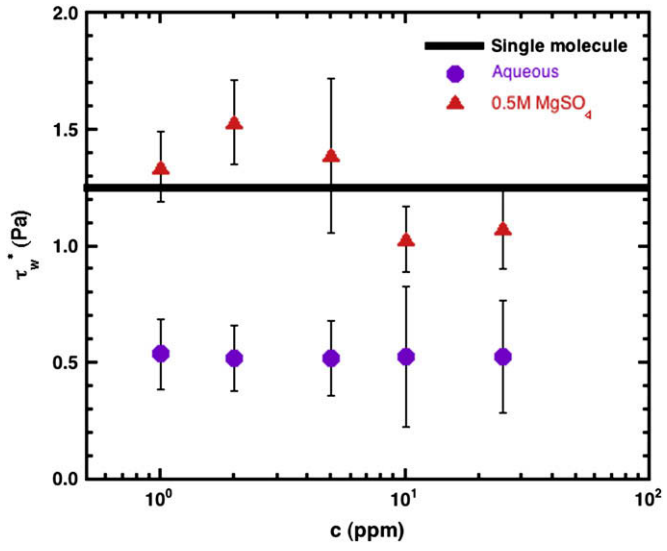

Fig. 8. Comparison of the onset wall shear stress for turbulent drag reduction, τ_w^*, for WSR 301 with 0.5 M $MgSO_4$ and in pure aqueous solution. The horizontal line is the onset stress prediction given by Virk for PEO, based on single molecule physics, computed as discussed in the text.

Thus, we conclude that: (i) addition of salt modulates the aggregate structure of WSR-301. Several classic PEO/salt SANS studies support this claim [64–66] in addition to our DLS results; (ii) This modulation is directly correlated to the drag reduction behavior of WSR-301. By linking molecular and macro scale observations, the combination of turbulent drag reduction data (Figs. 7 and 8) and DLS characterization of the polymer solutions (Figs 3, 4 and 5) establishes that aggregate structure plays a significant role in the turbulent drag reduction of high molar mass PEO.

4. Discussion

The principal result of the DLS studies is that the effective size of high molar mass PEO in aqueous solution is too large for center-of-mass diffusion to be probed in a wide-angle light scattering device. The scaling of the relaxation rate, Γ, with q^3 observed is reminiscent of the pioneering work of Adam and Deslanti [53], in which internal fluctuations of a large polystyrene chain were probed in benzene. Because the bare hydrodynamic radius of a single molecule of WSR 301 PEO is too small to yield the result $\Gamma \sim q^3$ by itself, we propose that the scaling is due to the effects of aggregation.

However, this hypothesis raises a number of questions. For example, $\Gamma \sim q^3$ is a prediction of the Zimm model for internal coil motions [53] – it is valid for a Gaussian chain with hydrodynamic interactions. Fig. 9 addresses if the theoretical curve $\Gamma = 0.07kTq^3/\eta$ for the Zimm model can be applied to the case of aggregation. In the equation plotted, η is the solvent viscosity. (These data are as Fig. 4a and b; however, they are now replotted as Γ/q^2 to emphasize the deviation from center-of-mass diffusion, which would appear as a horizontal line in the figure.) It is clear from Fig. 9 that the PEO relaxation rate data obey the correct scaling as the internal fluctuation theory but fall below the predicted curve. This discrepancy in prefactor depends on the details of the polymer – we observe a different prefactor for the polydisperse, high molar mass WSR 301 ($A = 1.47 \times 10^{-18}$) than for the narrow polydisperse polymer of 1.2 M molar mass ($A = 2.67 \times 10^{-17}$). To our knowledge there is as yet no theory or simulation of dilute aggregate dynamics that would explain the correspondence between our measurements and those of Adam and Deslanti [53]. Yet, the correspondence is

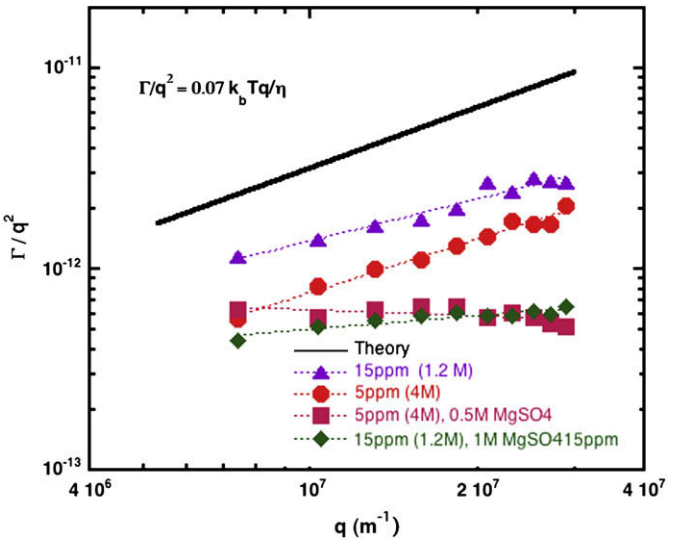

Fig. 9. Summary of DLS results, plotted as Γ/q^2 to emphasize the deviation from center-of-mass diffusion, for the two polymers and salts studied. The curve is the theoretical prediction for a Gaussian coil [53].

reasonable: Just as in a single Gaussian coil, for which the dynamics of the two chain ends contributes negligibly to the internal q^3 dynamics, so would the contacts between the multiple PEO molecules in an aggregated cluster be expected to negligibly affect internal dynamics. Then, because the internal dynamics of the Zimm model probed in the high q limit is independent of molar mass, dilute aggregate high q dynamics would be similar to the single-molecule prediction [67].

Fig. 2 measurements appear to disagree with previous DLS studies of dilute PEO dynamics that observed two relaxation rates, both of which scaled as q^2 [16,21,68]. In the present study a single dominant relaxation rate scaling as q^3 is observed. One difference in the studies is the concentration. Although all these studies are dilute ($c < c^*$), the earlier work of Duval et al. ($c/c^* > 0.1$) as well as Ho et al. ($c/c^* > 0.3$) are at greater concentration than our work (for which $0.001 < c/c^* < 0.08$). Moreover, Polverari et al. observed two peaks in their PEO DLS relaxation spectrum above a molecular weight dependent critical self-association concentration. If the self-association that leads to aggregation is viewed as a phase separation (akin to a micellization transition) in which single chains are in equilibrium with aggregate clusters, it seems likely that the ultra-dilute concentrations of this study render the concentration of single chains so small as to be undetectable by DLS. Thus, the observation of single relaxation behavior here is not inconsistent with the earlier studies, but instead is explained by the ultra-dilute concentration range studied. (These ultra-dilute concentrations are exactly the ones of interest for applications such as turbulent drag reduction.)

DLS experiments at a higher, but still dilute, concentration (100 ppm WSR 301: $c/c^* = 0.16$) confirm this explanation because two peaks in the DLS relaxation spectrum were observed (data not shown). Thus, we conclude that at ultra-low concentrations ($c/c^* < 0.1$), PEO quiescent dynamics is dominated by the behavior of aggregate clusters.

Although the quiescent dynamics of high molar mass PEO is dominated by the effect of polymer aggregates, the analysis of the drag reduction measurements of Fig. 8 also supports a role for flow-induced de-aggregation in turbulent flow. For example, although the shift in drag reduction onset condition (and therefore viscoelastic relaxation time) upon addition of $MgSO_4$ is too great to be explained as a simple effect of solvent quality, the apparent molar mass for WSR-301 extracted by application of Virk's well-established phenomenology is $\sim 7 \times 10^6$ g/mol, a number that is reasonably explained by single-molecule ideas. A probable explanation of the difference between the quiescent DLS and the turbulent results is the effect of flow-induced degradation. Here two possibilities should be considered. The first is single-chain scission due to covalent bond breakage. The second is PEO aggregate degradation due to rupture of intermolecular associations mediated by, for example, hydrogen bonding [69].

Polymer chain scission is typically apparent in Prandtl–von Karman plots such as Fig. 7 as deviation at high $Re f^{0.5}$ from Eq. (2). The deviation results in a maximum in $f^{-0.5}$ with further decline as $Re f^{0.5}$ increases [48,70]. Furthermore, the onset of these deviations can be quantitatively predicted by the Kolmogorov cascade theory of turbulent chain scission by Vanapalli et al. [71]. By considering these two effects below, we conclude that the measurements here are not affected by single chain scission.

First, we observe no deviation from Eq. (2) in the Prandtl–von Karman plots (Figs. 6 and 7). Indeed, Vanapalli et al. have shown that for PEO with mean molar mass of about 4×10^6 g/mol, polymer scission affects the drag reduction curves only for $(Re\sqrt{f})$ values greater than ~ 1000 [48], much larger than the values probed in this study. Second, application of the Kolmogorov cascade scission theory given the covalent bond strength of PEO (~ 4.1 nN [71]) yields an expected onset of covalent scission for $(Re\sqrt{f}) \sim 2300$, well above the range of our measurements. This estimate is given by $F_{max} \sim \pi\mu^2 Re^{3/2} L^2/4\rho d^2 \ln(L/a)$ where $F_{max} = 4.1$ nN, μ is the viscosity, Re is the Reynolds number, ρ is the fluid density, d is a characteristic geometric dimension of the flow, a is a characteristic radius of the polymer chain and L is the contour length of the polymer chain [71]. Thus, polymer molar masses in the range of $4–7 \times 10^6$ g/mol are unlikely to undergo chain scission (covalent bond breakage) in the turbulent flows studied. Instead, the quiescent aggregate structure quantified by the DLS does not appear to fully survive the turbulent flow.

Even though some flow-induced de-aggregation is observed, because the addition of salt significantly reduces the measured turbulent drag reduction in a way that cannot be explained by simple solvent effects, the differences in Figs. 7 and 8 are due to the effect of salt on residual aggregate structure. If the aggregate hypothesis is correct, we can estimate a lower bound on the size of the PEO aggregates studied because Adam and Delsanti [53] found q^3 scaling for measurements on single chains provided $qR_g > 4.4$. This constraint yields a lower bound for $R_{g,agg} \sim 740$ nm for the polymers studied here. Improving this estimate should be a principal aim of future work.

Small-angle dynamic light scattering [72] could be applied to characterize the size of PEO aggregates at ultra-dilute conditions. The dynamic response of a dilute polymer solution can be divided into different regimes based on the magnitude of the dimensionless scale qR_h, where R_h is the hydrodynamic radius of the polymer and q is the scattering wave vector. In a sufficiently small q limit, the dynamic light scattering spectra of dilute PEO solutions should be consistent with center-of-mass diffusion of multi-molecule aggregates with an effective hydrodynamic radius that is many times greater than the hydrodynamic response of a single molecule of PEO. In the high q limit internal dynamics is probed, as per Fig. 2. The transition between the two dynamical regimes occurs at $qR_{agg} \sim 1$. Given estimates from this study, R_{agg} could be as large as 740 nm. Thus a DLS device that can probe $q \ll 1.33\ \mu m^{-1}$ is required, corresponding to $\theta \ll 6°$. Such small-angle DLS instruments have become available [72,73].

5. Conclusions

This work addresses the problem of PEO aggregation in aqueous solution by building upon the earlier work of Polverari et al., Hammouda et al., and Liberatore et al. [16,19,25,38,39]. The current

study uses a unique chaotropic/inorganic salt and simultaneous dynamic light scattering/fluid dynamics methodology to study dilute PEO aggregate flow properties. We find:

(1) The DLS relaxation spectra of high molar mass dilute aqueous PEO solutions show a single peak that scales as $\Gamma \sim q^3$, where Γ is the relaxation rate and q is the scattering vector. This scaling is consistent with DLS detection of internal fluctuations of a polymer aggregate of size at least 740 nm.
(2) Addition of an inorganic ($MgSO_4$) or chaotropic salt (GuS) decreases the power law of the relaxation rate scaling from q^3 to q^2. This shift from a scaling indicative of aggregate dynamics ($\Gamma \sim q^3$) to one characteristic of polymer center-of-mass diffusion ($\Gamma \sim q^2$) shows that these salts are effective de-aggregation agents for PEO.
(3) The DLS results are predictive of the behavior of PEO in turbulent flow. Addition of $MgSO_4$ significantly decreases the effectiveness of PEO as a drag reduction agent. The effect is greater than can be explained by the role of solvent quality effects. The level of drag reduction observed when compared to the DLS measurements suggests that turbulent flow de-aggregates high molar mass PEO, even in mild flow systems with shear stresses ~ 0.5 Pa.

These results improve our fundamental understanding of the behavior of dilute solutions of high molar mass PEO by placing bounds on the size of quiescent aggregates, by demonstrating the effect of salt on aggregate structure and by linking aggregate structure to flow behavior of PEO.

Acknowledgments

We thank Siva Vanapalli for valuable discussions.

Appendix

A general equation to correlate the drag reduction behavior for a polymer is [34]:

$$\frac{1}{\sqrt{f}} = (4+\delta)\log_{10}\left(\mathrm{Re}\sqrt{f}\right) - 0.4 - \delta\log_{10}\left(\left(\mathrm{Re}\sqrt{f}\right)^*\right) \qquad (2)$$

Here δ is the slope increment which quantifies the difference in the slopes of the polymer solution and the Newtonian solvent drag reduction curves on a Prandtl–von Karman plot. The slope increment increases both with increasing polymer concentration and polymer molecular weight. $(\mathrm{Re}\sqrt{f})^*$ is the value of $(\mathrm{Re}\sqrt{f})$ at the onset of drag reduction. It is the point where the polymer drag reduction curve intersects the Prandtl–von Karman curve. Note that $(\mathrm{Re}\sqrt{f})^*$ is simply related to the onset condition, τ_w^* through the following equations:

$$\left(\mathrm{Re}\sqrt{f}\right)^* = \frac{\sqrt{2}u_\tau^* d}{\nu_s} \quad \text{where } u_\tau^* = \sqrt{\frac{\tau_w^*}{\rho}} \qquad (3)$$

In the above equations u_τ^* is the onset pipe friction velocity and d is the diameter of the pipe used for the study. Note that knowledge of the onset condition and slope increment specifies the turbulent drag reduction of a polymer in turbulent flow in a pipe of a particular diameter. Generally, τ_w^* and delta are both the function of polymer molar mass (and/or aggregate structure). δ is also a function of the polymer concentration with a typical dependence of $\delta \sim c^{1/2}$ observed [34].

In addition, the critical Weissenberg number, a universal criterion for the onset of turbulent drag reduction is defined as $Wi^* = \lambda\tau_w^*/\mu$. Virk has shown that Wi^* is a constant for all drag reduction flows and is given by $Wi^* = 5.5K_\lambda/H$, where K_λ is the width of the relaxation time spectrum for the polymer and H is the heterogeneity index of the polymer. This discussion anticipates the potential relationship between onset of turbulent drag reduction and aggregate structure. Aggregation will affect the viscoelastic relaxation time of the dilute polymer solution. This effect will shift the onset condition for turbulent drag reduction because onset is controlled by a critical Wi^*. For the PEO samples used in this study, we compute $Wi^* = 1.6$, from Virk.

References

[1] Baghdadi HA, Sardinha H, Bhatia SR. Journal of Polymer Science, Part B: Polymer Physics 2005;43(2):233–40.
[2] Morgan SE, McCormick CL. Progress in Polymer Science 1990;15(1):103–45.
[3] Gil ES, Hudson SA. Progress in Polymer Science 2004;29(12):1173–222.
[4] Figueredo RCR, Sabadini E. Colloids and Surfaces A: Physicochemical and Engineering Aspects 2003;215(1–3):77–86.
[5] Kauser N, Dos Santos L, Delgado M, Muller AJ, Saez AE. Journal of Applied Polymer Science 1999;72(6):783–95.
[6] Rodriguez S, Romero C, Sargenti ML, Muller AJ, Saez AE, Odell JA. Journal of Non-Newtonian Fluid Mechanics 1993;49(1):63–85.
[7] Addai-Mensah J, Yeap KY, McFarlane AJ. Powder Technology 2007;179(1–2):79–83.
[8] Toryanik AI. Journal of Structural Chemistry 1984;25(3):385–8.
[9] Dormidontova EE. Macromolecules 2002;35(3):987–1001.
[10] Straziel C. Makromolekulare Chemie: Macromolecular Chemistry and Physics 1968;119(DEC):50–63.
[11] Saeki S, Kuwahara N, Nakata M, Kaneko M. Polymer 1976;17(8):685–9.
[12] Malcolm GN, Rowlinson JS. Transactions of the Faraday Society 1957;53(7):921–31.
[13] Dormidontova EE. Macromolecules 2004;37(20):7747–61.
[14] Smith GD, Bedrov D, Borodin O. Physical Review Letters 2000;85(26):5583.
[15] Tasaki K. Journal of the American Chemical Society 1996;118(35):8459–69.
[16] Polverari M, vandeVen TGM. Journal of Physical Chemistry 1996;100(32):13687–95.
[17] Kalashnikov VN. Journal of Polymer Science, Part B: Polymer Physics 1999;37(22):3208–16.
[18] Cunibert C, Ferrando R. Polymer 1972;13(8):379–84.
[19] Hammouda B, Ho D, Kline S. Macromolecules 2002;35(22):8578–85.
[20] Cuniberti C. Polymer 1975;16(4):306–7.
[21] Duval M, Sarazin D. Polymer 2000;41(7):2711–6.
[22] Berne BJ, Pecora R. Dynamic light scattering. New York: J Wiley; 1976.
[23] Polik WF, Burchard W. Macromolecules 1983;16(6):978–82.
[24] McIntyre D, Gornick F. Light scattering from dilute polymer solutions. New York: Gordon and Breach Science Publishers; 1964.
[25] Hammouda B, Ho DL, Kline S. Macromolecules 2004;37(18):6932–7.
[26] Vlassopoulos D, Schowalter WR. Journal of Rheology 1994;38(5):1427–46.
[27] Kalashnikov VN. Journal of Rheology 1994;38(5):1385–403.
[28] Tirtaatmadja V, McKinley GH, Cooper-White JJ. Physics of Fluids 2006;18(4).
[29] Choi HJ, Jhon MS. Industrial and Engineering Chemistry Research 1996;35(9):2993–8.
[30] Berman NS. Annual Review of Fluid Mechanics 1978;10:47–64.
[31] Berman NS. Physics of Fluids 1977;20(5):715–8.
[32] White CM, Mungal MG. Annual Review of Fluid Mechanics 2008;40:235–56.
[33] Larson RG. Journal of Rheology 2005;49(1):1–70.
[34] Virk PS. Aiche Journal 1975;21(4):625–56.
[35] Dunlop EH, Cox LR. Physics of Fluids 1977;20(10):S203–13.
[36] Vlachogiannis M, Liberatore MW, McHugh AJ, Hanratty TJ. Physics of Fluids 2003;15(12):3786–94.
[37] Liberatore MW, Baik S, McHugh AJ, Hanratty TJ. Journal of Non-Newtonian Fluid Mechanics 2004;123(2–3):175–83.
[38] Liberatore MW, Pollauf EJ, McHugh AJ. Journal of Non-Newtonian Fluid Mechanics 2003;113(2–3):193–208.
[39] Liberatore MW, McHugh AJ. Journal of Non-Newtonian Fluid Mechanics 2005;132(1–3):45–52.
[40] Shin M, Shaqfeh ESG. Centre for Turbulence Research. Annual Research Briefs; 2005. p. 389.
[41] Little RC. Journal of Applied Polymer Science 1971;15(12):3117–25.
[42] Little RC, Patterso RI. Journal of Applied Polymer Science 1974;18(5):1529–39.
[43] Yuan GC, Wang XH, Han CC, Wu C. Macromolecules 2006;39(18):6207–9.
[44] Lim ST, Hong CH, Choi HJ, Lai PY, Chan CK. Europhysics Letters 2007;80(5):58003.
[45] Boom R, Sol CJA, Salimans MMM, Jansen CL, Wertheimvandillen PME, Vandernoordaa J. Journal of Clinical Microbiology 1990;28(3):495–503.
[46] Vanapalli SA. PhD thesis. Department of Chemical Engineering, University of Michigan; 2006.
[47] Hunston DL, Reischman MM. Physics of Fluids 1975;18(12):1626–9.
[48] Vanapalli SA, Islam MT, Solomon MJ. Physics of Fluids 2005;17(9).
[49] Draad AA, Kuiken GDC, Nieuwstadt FTM. Journal of Fluid Mechanics 1998;377:267–312.

[50] McKeon BJ, Smits AJ. Measurement Science and Technology 2002;13(10):1608–14.
[51] Provencher SW. Computer Physics Communications 1982;27(3):229–42.
[52] Devanand K, Selser JC. Macromolecules 1991;24(22):5943–7.
[53] Adam M, Delsanti M. Macromolecules 1977;10(6):1229–37.
[54] Sun T, King HE. Macromolecules 1996;29(9):3175–81.
[55] Amis EJ, Han CC. Polymer 1982;23(10):1403–6.
[56] Eisele M, Burchard W. Macromolecules 1984;17(8):1636–8.
[57] Harnau L, Winkler RG, Reineker P. Journal of Chemical Physics 1996;104(16):6355–68.
[58] Matsuoka H, Morikawa H, Yamaoka H. Colloids and Surfaces A: Physicochemical and Engineering Aspects 1996;109:137–45.
[59] Boyko V, Richter S, Burchard W, Arndt KF. Langmuir 2007;23(2):776–84.
[60] Rubinstein M, Colby RH. Polymer physics. Oxford University Press; 2004.
[61] Sureshkumar R, Beris AN, Handler RA. Physics of Fluids 1997;9(3):743–55.
[62] Sreenivasan KR, White CM. Journal of Fluid Mechanics 2000;409:149–64.
[63] Dimitropoulos CD, Sureshkumar R, Beris AN. Journal of Non-Newtonian Fluid Mechanics 1998;79(2–3):433–68.
[64] Hakem IF, Lal J, Bockstaller MR. Journal of Polymer Science, Part B: Polymer Physics 2006;44(24):3642–50.
[65] Hakem IF, Lal J, Bockstaller MR. Macromolecules 2004;37(22):8431–40.
[66] Hakem IF, Lal J. Europhysics Letters 2003;64(2):204–10.
[67] Doi M, Edwards SF. The theory of polymer dynamics. Oxford: Clareendon Press; 1986.
[68] Ho DL, Hammouda B, Kline SR. Journal of Polymer Science, Part B: Polymer Physics 2003;41(1):135–8.
[69] Horn AF. Nature 1984;312(5990):140–1.
[70] Elbing BR, Winkel ES, Solomon MJ, Ceccio SL, submitted for publication.
[71] Vanapalli SA, Ceccio SL, Solomon MJ. Proceedings of the National Academy of Sciences of the United States of America 2006;103(45):16660–5.
[72] Cipelletti L, Weitz DA. Review of Scientific Instruments 1999;70(8):3214–21.
[73] Ferri F. Review of Scientific Instruments 1997;68(6):2265–74.